Final Draft
of the original manuscript:

Daudin, R.; Terzi, S.; Mallmann, C.; Sanchez Martin, R.; Lhuissier, P.;
Boller, E.; Pacureanu, A.; Katsarou, L.; Dieringa, H.; Salvo, L.:
Indirect improvement of high temperature mechanical properties of a Mg-based alloy Elektron21 by addition of AlN nanoparticles
In: Materials Science and Engineering A (2017) Elsevier

DOI: 10.1016/j.msea.2017.01.103

Indirect improvement of high temperature mechanical properties of a Mg-based alloy Elektron21 by addition of AlN nanoparticles

R. Daudin[1], S. Terzi[2], C. Mallmann[1], R. Sánchez Martín[3], P. Lhuissier[1], E. Boller[4], A. Pacureanu[4], L. Katsarou[5], H. Dieringa[5], L. Salvo[1]

[1]Univ. Grenoble Alpes, CNRS, SIMaP, F-38000 Grenoble, France
[2]European Space Agency, ESTEC, TEC-TS, EPN Campus, CS20156, 38042 Grenoble Cedex 9, France
[3]IMDEA Materials Institute Tecnogetafe C/ Eric Kandel, 2 28906 Getafe (Madrid), Spain
[4]European Synchrotron Radiation Facility, 71 Avenue des Martyrs, 38000 Grenoble, France
[5]Helmholtz-Zentrum Geesthacht, Magnesium Innovation Centre – MagIC, Max-Planck-Str. 1, 21502 Geesthacht, Germany

Keywords: Metal matrix composites, Mechanical properties, Tomography, AlN nanoparticles

Abstract

Magnesium being the lightest metal on earth used as a structural material, the design of the chemistry and the microstructures of Mg-based alloys has been developed over the years to always further ameliorate their mechanical properties. A supplementary option consists in adding ceramic nanoparticles to such alloys to design Mg-based metal matrix nanocomposites (MMNCs) displaying improvement of both strength and ductility. In practice however, careful attention is required to understand the fundamental mechanisms at the heart of the enhancement of these properties as they still remain quite uncertain and subjected to misleading interpretations. Here, high temperature (350°C) strain rate jump tests in compression reveal an enhancement of 20 to 60 % of the mechanical properties when AlN nano-particles are added to the Elektron 21 alloy (Mg-2.8Nd-1.2Gd-0.4Zr-0.3Zn, in wt%). At the same time, nano-indentation investigations suppose that forest or Orowan strengthening, due to particles-dislocations interactions, is unlikely to occur. Instead, using complementary microstructural characterization techniques (scanning electron macroscopy, energy dispersive spectroscopy as well as micro- and nano-tomography), we show that AlN nano-particles physically and chemically interact with the alloy and modify the overall microstructure, in particular the intermetallic phase, at the origin of the improvement of the mechanical properties.

1. Introduction

In the current context of energy saving, such as in the transportation sector, magnesium, the lightest metal used as structural material, is becoming more and more attractive to replace heavier materials. Over the years, numerous Mg-based alloys have been designed to fit various application constrains [1]. Among them, the AM (Mg-Al-Mn) and the AZ (Mg-Al-Zn) series are widely used in everyday products as they present good resistance to corrosion and good mechanical properties at room temperature at relatively low cost. For applications operating at higher temperature, Mg-based alloys free of aluminium and containing rare earth

elements (Mg-RE) are known to exhibit relatively fair creep resistance but strengthening magnesium above 200°C only by alloying remains a challenge [2]. A complementary route consists in strengthening Mg and Mg-based alloys by the addition of ceramic particles to obtain Metal Matrix Composites (MMC) [3]. Such addition theoretically results in different strengthening mechanisms arising either from the physical presence of particles: Orowan strengthening (dislocations bowing on particles) and Hall-Petch strengthening (grain refinement), or from the different properties of the particles and the metal matrix: forest strengthening (due to different thermal coefficients) and Taylor strengthening (due to different Young's modulus) [4–8].

With the emergence of novel nanosized ceramics particles and the development of processing techniques to prevent their natural agglomeration in the melt, the MMNCs have arisen and been developed more recently [5,6,9–12]. The advantage of using ceramic particles of very small size is the possibility to enhance the grain refinement processes as well as the forest strengthening [13] mechanisms by adding only a very small amount of reinforcers (typically 1wt%) and without detrimental impact on the ductility [14,15]. Such a relatively low amount of particles inside the alloys allows the weight and the cost of this promising materials to remain low and therefore attractive for industrial applications. Concerning Mg-based MMNCs, additions of Y_2O_3, ZrO_2, SiC, Al_2O_3 and AlN nano-particles are reported to increase the Mg-alloy mechanical properties in different extents [15–18]. The challenge of the European project ExoMet was to design and investigate the mechanical response and the microstructure of several selected MMNCs [19]. Among the various matrix/nano-particles combinations considered in this project, the addition of AlN nano-particles (~25 nm in diameter) into the Mg-alloy Elektron21 was found to significantly improve the creep properties. Elektron21 (El21) is a Mg-2.8Nd-1.2Gd-0.4Zr-0.3Zn (wt%) alloy [20–22]. The addition of neodynium helps to improve the tensile strength at high temperature as well as to reduce residual porosity while gadolinium, in combination with zinc, further enhance the mechanical properties throughout precipitation strengthening mechanisms. Zirconium is very stable toward the other components and is used as grain refiner [1,20,23,24]. The El21+AlN nano-composites designed in the framework of the ExoMet project has already been reported in [25] and was shown to present higher creep resistance compared to the unreinforced alloy. However, the fundamental role of the particles and the key mechanisms affecting the mechanical properties are not yet totally unravelled. Indeed the precise location of the nano-particles [26], their potential reactions with the alloying elements [25,27], their behaviour during casting [19] as well as their true impact on the different strengthening mechanisms [5] are still important open questions requiring investigations in order to fully grasp the modification of the mechanical properties.

The present paper compares the mechanical behaviours at high temperature and the microstructures of the El21 alloy processed on the one hand without particle and on the other hand with the addition of AlN nanoparticles. It aims to provide significant complementary information to the recent paper of Katsarou *et al* [25] which investigated the same materials using mechanical creep tests and transmission electron microscopy (TEM). To do so, compression tests at high temperature as well as nano-hardness at room temperature were carried out. Complementary structural characterization techniques (X-ray micro-tomography,

Scanning Electron Macroscopy (SEM), Energy Dispersive Spectroscopy (EDS) and X-ray nano-holotomography) were used to gain insights, with a larger field of view compared to TEM [25], about the influence of the nano-particles on the local as well as on the overall modification of the microstructure at the origin of the difference of the mechanical responses.

2. Experimental

2.1. Materials processing

The Elektron21 alloy was processed at the Helmholtz-Zentrum Geesthacht where it was melted and kept in the liquid state at 670°C. 1 wt% of AlN particles (25 nm) was then added to the melt which was subsequently stirred (200 rpm) and ultrasonically processed with a Ti sonotrode for 5 min at 0.3 kW. The material was then solidified by placing the mould containing the melt into a water bath. For reference, an El21 alloy sample without particle was processed exactly the same way. The complete processing procedure can be found elsewhere [19,25].

2.2. High temperature compression tests

The compression tests at high temperature were performed at Grenoble at the SIMaP laboratory where the samples were machined into cylindrical-shape specimens of 4.5 mm in length and 3 mm in diameter. Each sample was placed with its main axis perpendicular to the surface of the lower arm of the machine. The heating rate to reach a temperature of 330 °C in the furnace mounted on the compression device was set to 16.5 °C.min^{-1}. To avoid thermal overshoot in the sample the heating rate was reduced to 10 °C.min^{-1} to reach the operating temperature of 350°C. Five more minutes at 350°C were assumed to be necessary to ensure a good thermal homogeneity in the sample before launching the tests. Different strain rates were applied during the same tests to characterize the mechanical behaviour at high temperature. The imposed strain rates as a function of the strain values are listed in the table in Figure 1. After completion of the tests, the furnace was open and the sample was removed and quenched in water.

2.3. Nano-Hardness

The nano-hardness measurements were carried out at IMDEA laboratory in Madrid. The sample preparation for microstructural and nanoindentation characterisation included surface grinding using 1200 and 2000 grit size SiC papers, followed by mechanical polishing with 3 and 1 µm diamond paste. A final polishing mechanical step was performed using an OP-S colloidal silica solution. Individual grains in EL21 alloy samples with and without AlN nanoparticles were indented following the protocol described in Figure 2(a). The hardness was measured at 5 different points located at a distance from the eutectic regions of 10, 20, 30, 40 and 50 µm respectively. Two different indentations, separated by 10 µm, were carried out per distance. The indentations were performed using a Hysitron TI 950 TriboIndenter system fitted with a Berkovich tip in displacement control mode with a maximum depth of 500 nm. A trapezoidal loading curve, with a loading and unloading time of 5 s and a dwell time of 2 s at maximum depth, was chosen for all the indentation procedures.

2.4. X-ray micro- and nano-tomography

X-ray tomography characterization of the EL21 alloy unreinforced or reinforced with AlN nanoparticles has been carried out at room temperature, at the European Synchrotron Radiation Facility (ESRF) on two beamlines. Conventional absorption tomography scans were performed on ID19 with a pixel size of 0.55 µm and a CMOS PCO-Dimax camera (field of view 2016 x 2016 pixels). On the ID16A beamline, scans at four different focus-to-sample distances were recorded to perform holo-tomography that takes phase contrast into account [28] with a pixel size of either 100 nm or 25 nm and with a CCD FreLoN camera (field of view 2048 x 2048 pixels). On ID19 a pink beam of 17.6 keV was used and 800 projections have been taken over 180°, while an energy of 33.6 keV was used on ID16A and 2000 projections (over 360°) were taken with an exposure time of 0.5 s. The micro-tomography scans were reconstructed using filtered back projection algorithms using the conventional ESRF PyHST software package. Nano-holotomography scans required phase field retrieval processes prior to reconstruction. The reconstructed 3D images were then treated and analysed using conventional imaging software such as ImageJ.

3. Results and discussion

3.1. Mechanical characterization results

Figure 1(a) compares the strain-stress curves recording during the compression tests with imposed strain rate jumps at 350°C. A strain rate of 10^{-3} s^{-1} was imposed two times during the same test ($\varepsilon \in [0 - 0.1]$ and $\varepsilon \in [0.2 - 0.25]$). For both samples, similar stress values (52±2 MPa for El21 without particles and 83±1 MPa for El21 with AlN particles) were recorded for this specific strain rate ensuring that no residual stress that could influence the results are present in the samples. These curves clearly show that the addition of only 1wt% of AlN particles in the El21 alloys successfully enhances the mechanical properties at high temperature. Indeed an improvement of the stress response from 20% at large strain rates to more than 60% at low strain rates is measured. The results are in very good agreement with the improvement of creep published in [25] for the same materials. At high temperature, the deformation mechanisms can be represented by the following relationship:

$$\dot{\varepsilon} = A \frac{DGb}{k_B T} \left(\frac{\sigma}{E}\right)^n \left(\frac{b}{d}\right)^p \quad (1)$$

where A is a dimensionless constant, k_B the Boltzmann constant, T the temperature, D the diffusion coefficient, G the shear modulus, b the Burger vector, d the mean grain size, E the Young´s modulus, p the inverse grain size sensitivity exponent and n the Norton exponent.

ε	0-0.1	0.1-0.15	0.15-0.2	0.2-0.25	0.25-0.3	0.3-0.35	0.35-0.4	0.4-0.45	0.45-0.5
$\dot{\varepsilon}$ (10^{-3} s^{-1})	1	0.2	0.4	1	0.8	2	4	8	10

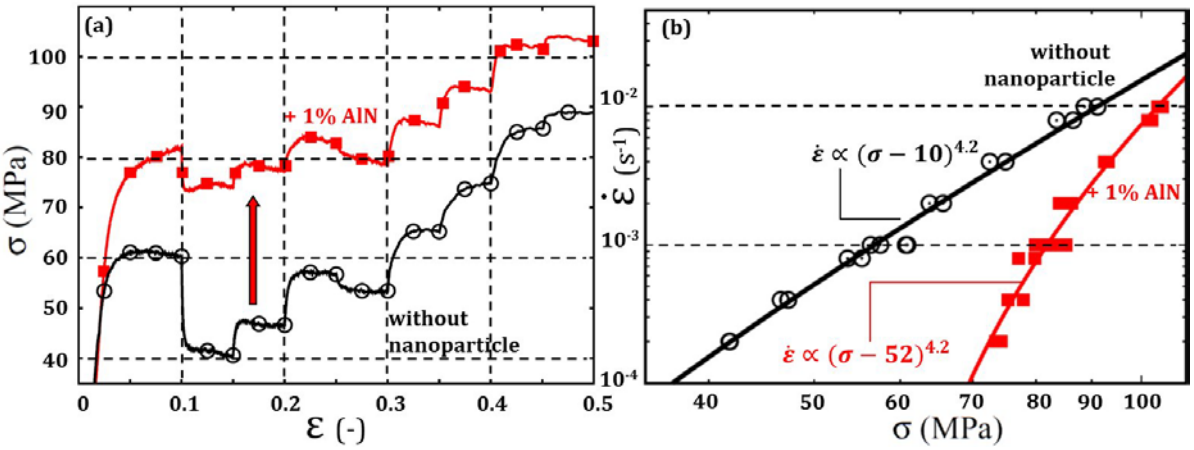

Figure 1 : (a) Strain-stress curves obtained during the compression tests with strain rates jumps at 350°C for the El21 without particles (black-circles) and the El21+AlN particles (red-squares). The table above gives the applied strain rates corresponding to the strain states. (b) log-log plots of strain rates as a function of stress values extracted from the mean values of the plateau on the stain-stress curves. Dots are experimental data while lines show the best fit obtained (see text).

The Norton exponent n is related to the physical processes driving the deformation. Values ranging from 3 to 5 correspond to dislocation-controlled mechanisms occurring inside grains (both glide and climb) and values of 2 and below are related to diffusion-controlled mechanisms such as grain boundary sliding. A log-log plot of $\dot{\varepsilon} = f(\sigma)$ using the experimental data allows n to be determined (Figure 1(b)). In the present case, one can observe that the experimental points for the El21 sample without particle spread out on an almost straight line while for the El21+AlN particles, the data lay on a curved line highlighting a stress dependence of the stress exponent. Such behaviour could only be fitted using the concept of the threshold stress (σ_{thr}) assuming the appearance a of a resistive stress [29] that develops into the material due to the presence of particles. Such protocol was applied in [25] on both materials resulting in an effective stress exponent of the order of 4.2 and threshold stress values of 10.3 and 30.1 for the El21 and El21+AlN samples, respectively. Here, replacing σ by (σ-σ_{thr}) in equation (1) and fitting the experimental data points with the parameters of [25] gives a very good agreement for the El21 samples while a larger threshold stress value (σ_{thr} = 52 MPa) is found in the case of the El21+AlN sample (Figure 1(b)). The present valuable data however expand the validity domain (to higher strain rates) of the mechanical law used to describe the materials deformation at high temperature. The n value of 4.2 indicates that the movements of dislocations is the rate-controlling deformation mechanism and the rise of a significant threshold stress, even larger than in [25], indicates that dislocation movements at high temperature must be altered when AlN particles are added to the El21 alloy.

The origin of the threshold stress in MMNCs is claimed to be similar to precipitation hardening mechanisms due to the presence of immobile particles impeding the movement of dislocations [29–33]. To study such effects, nano-hardness measurements were carried out

inside the Mg-matrix grain and close to the intermetallic regions to assess possible hardening effects of the AlN particles (Figure 2). Surprisingly, the Mg-matrix grains in the El21+AlN nanocomposite display local hardness values always lower than in the El21 sample without particle suggesting that hardening of the Mg matrix by AlN reinforcements is unlikely to occur, in agreement with TEM investigations [25].

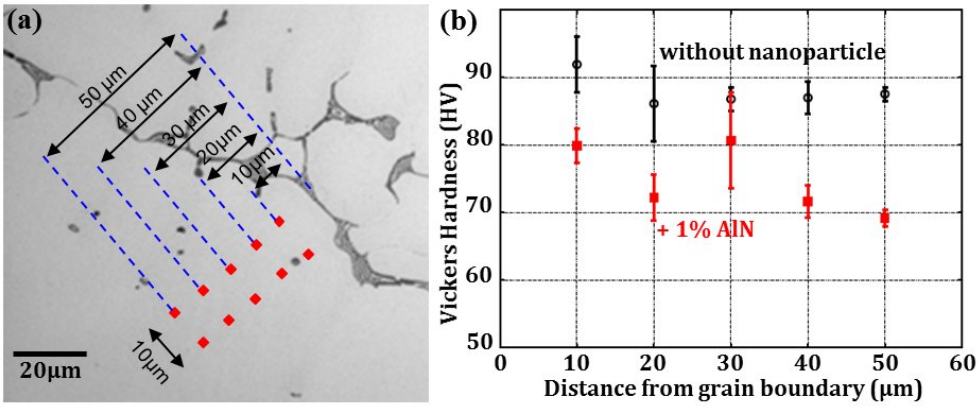

Figure 2: (a) Optical micrograph illustrating the nano-hardness measurements from the inner to the outer part of the grain. (b) Vickers hardness values as a function of the distance from the grain boundary for the El21 without particles (black-circles) and El21+AlN particles (red-squares).

The nano-indentation study thus shows that the motion of the dislocations is not influenced by the presence of particles in the grain nor by the rare-earth precipitates revealed by TEM [25]. However, the local hardness between the inner and the outer part of the grains (close to the intermetallic phase) increases by 14 % for the El21+AlN nanocomposite but only by 6 % for the El21 sample without particles. The intermetallic phase as well as the behaviour of the particles during casting and their location must be studied in more details. Indeed the presence of particles can also modify the matrix by interfacial reactions [34] during elaboration that may induce specific precipitation [25]. They can also influence the dendrites growth and thus modify the overall final microstructure leading to different mechanical properties.

3.2. *Microstructure characterization results:*

Figure 3 (a) and (b) are 2D images extracted from the room temperature micro-tomography 3D images. The Mg matrix is in grey whereas the intermetallic phase is in white. The scale is identical in both slices. It can first be mentioned that the processing of the El21+AlN nanocomposite is successful in the way that no detectable significant amount of porosity is revealed in the material. Indeed, defects such as pores are highly detrimental for mechanical properties and are one of the main difficulties to avoid in casting MMNCs [3]. This issue appears to be more problematic in Al-based than in Mg-based nanocomposites for which wettability between the Mg melt and ceramics particles is favourable. Moreover, it appears clearly that the intermetallic phase is different from one material to the other in terms of shape, distribution and thickness. The intermetallic of the El21+AlN nanocomposite looks

more branched, thinner as well as more homogeneously distributed. However, a 2D visualization can be misleading as slices can look very different from one to another.

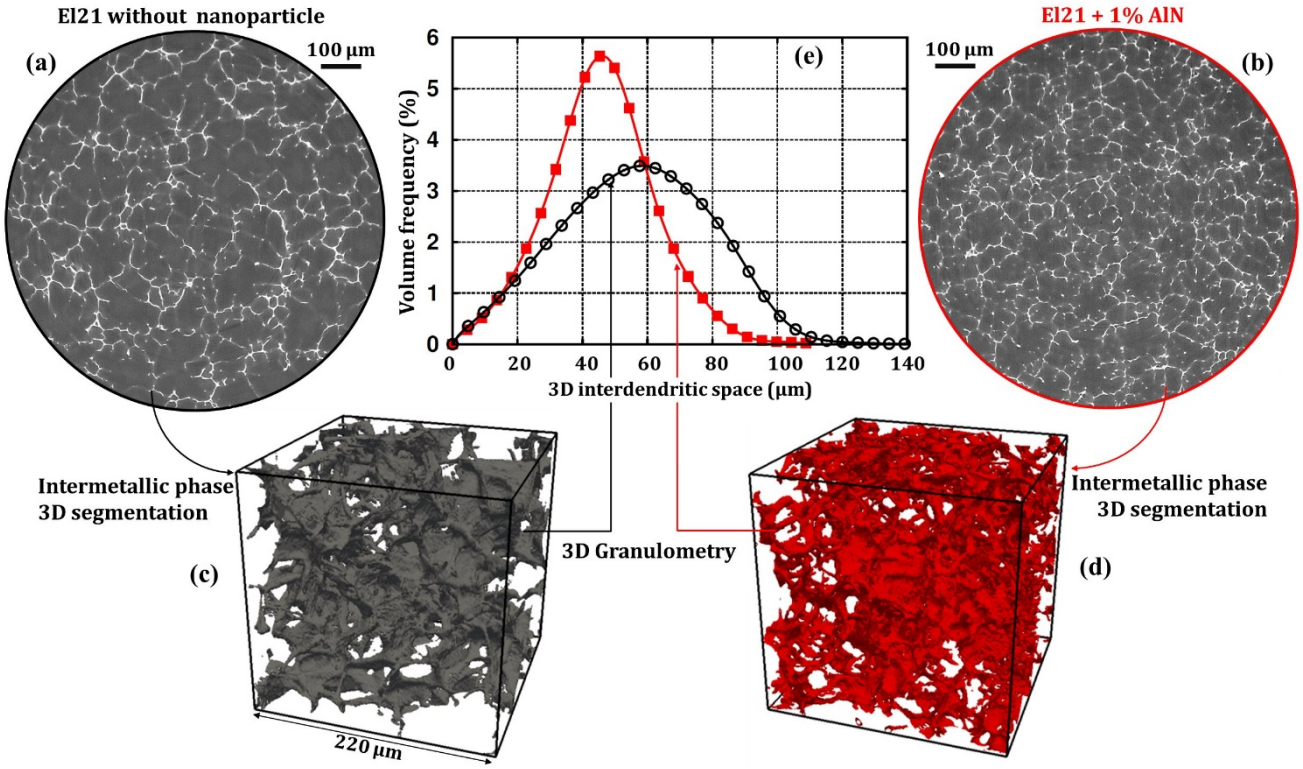

Figure 3 : Micro-tomography slice of (a) El21 without particles and (b) El21+Al nanocomposite (voxel size: 0.55 µm). The grey colours correspond to the matrix (i.e. the primary phase, mainly pure Mg) whereas white colours indicate the intermetallic phase (rare earth compounds) appearing at the end of the solidification and located at the grain boundaries. (c) and (d) show the 3D distributions of the intermetallic phase obtained from the segmentation of 100x100x100 μm^3 volumes of the El21 without and with AlN particles, respectively. (e) Mean 3D interdendritic space distribution obtained from 3D granulometry performed on the whole tomography volumes for the El21 without (black-circles) and with (red-squares) AlN particles.

To overcome this issue, a 3D characterization of the intermetallic shape and distribution was carried out. It consists in the segmentation of the intermetallic part. Examples of the resulting 3D information obtained are given by the intermetallic phase sub-volumes extracted from the overall volumes in both cases (Figure 3 (c) and (d)). Subsequently, a 3D granulometry analysis was performed, which allows one to extract the interdendritic space parameter (Figure 3(e)). In such plot, the position of the peak gives the mean value of the interdendritic space and the full width at half maximum (FWHM) gives the deviation from this value, i.e. information on the homogeneity of the intermetallic distribution. The interdendritic space distribution of the unreinforced El21 sample is broad and centred on 60 µm whereas for the El21+AlN the peak is sharper and centred on 48 µm. Interestingly Katsarou *et al.* also mentioned that the grain sizes between the two materials were comparable but their shape were different (the El21+AlN grains being more dendritic) which is here

confirmed with the 3D analysis of the interdendritic phase. The calculation of the intermetallic volume fractions yields 7.4 % and 6.0 % for the El21 and El21+AlN, respectively. Such very similar values imply that the specific surface of the intermetallic phase in the El21+AlN sample is much larger. As the intermetallic architecture is known to play a key role in the mechanical response of alloys [35], it seems very likely that the mechanical improvement is correlated to the 3D grain shape and therefore to the spatial intermetallic distribution: the more tortuous and homogeneously distributed the intermetallic phase is, the better the strengthening at high temperature.

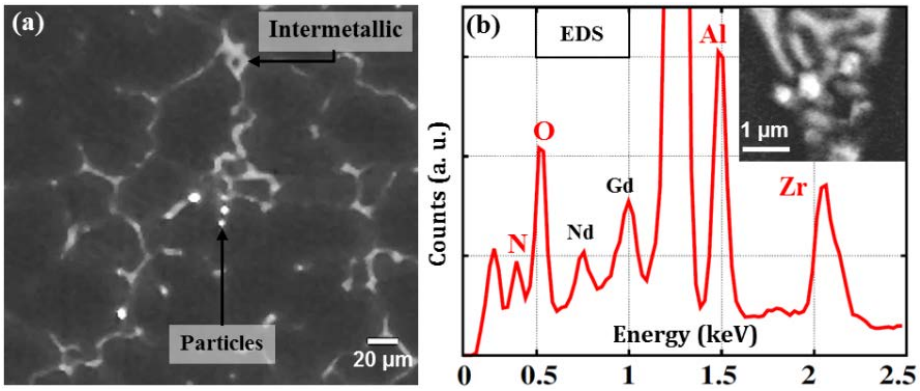

Figure 4: (a) 2D micro-tomography image showing the α-Mg primary phase (black), the intermetallic phase (grey) and some high absorbent particles (white). (b) Energy Dispersive Spectroscopy graph recorded on the white particles observed with a SEM located inside the intermetallic phase shown in inset.

The main drawbacks concerning micro-tomography images are the limited spatial resolution (basically 1.1 µm here) and the lack of unambiguous chemical analysis. Therefore, such resolution can only probe particles in the form of aggregates (and not isolated ones) and those that present an absorption coefficient relatively different from the other species present in the material which is not the case for AlN particles here. However, a closer look at the 3D images of the El21+AlN sample (Figure 4(a)) reveals the presence of intense bright spots that look like aggregates of particles located in the intermetallic phase. It has already been claimed that Al, whether in the form of free metallic phase material or in the form of AlN (or even Al_2O_3) particles, can react with other components, such as Zr, present in the El21 alloy [25,27,34]. Further investigations were thus performed by SEM imaging and EDS analysis (Figure 4(b)). First of all, small particle aggregates were again only found in the intermetallic area suggesting that they have been pushed by the solidification front and then entrapped between the dendrites arms. Second, the EDS chemical analysis revealed, in addition to Nd and Gd that composed the intermetallic, that Al and Zr (and few N) were the main components in such aggregates supporting the hypothesis of strong affinity between Al and Zr atoms that may interact and form compounds [36]. While spatial resolution as well as chemical information is gained using a SEM, there is always a chance of mislead interpretation as such technique cannot univocally probe a significant area, especially in 2D.

To complete the study, nano-holotomography acquisitions were performed to probe in 3D, at a very fine scale and with chemical insights, the 3D spatial distribution and the nature

of the particle present inside the El21+AlN nanocomposites after casting. In the 3D volumes recorded with a pixel size of 100 nm, no significant difference in the microstructures was observed in comparison with the micro-tomographic data. It however allowed regions of great interest to be selected to perform subsequent acquisitions with an even lower pixel size. Indeed, Figure 5 (a) and (b) are 2D slice extracted from a 3D volume acquired at a resolution of 25 nm per pixel and focus on areas of the intermetallic phase where aggregates of particles can be revealed. Such aggregates are not observed in the El21 sample without AlN supporting the fact that they originate from the addition of nanoparticles, nor in the α-Mg primary phase.

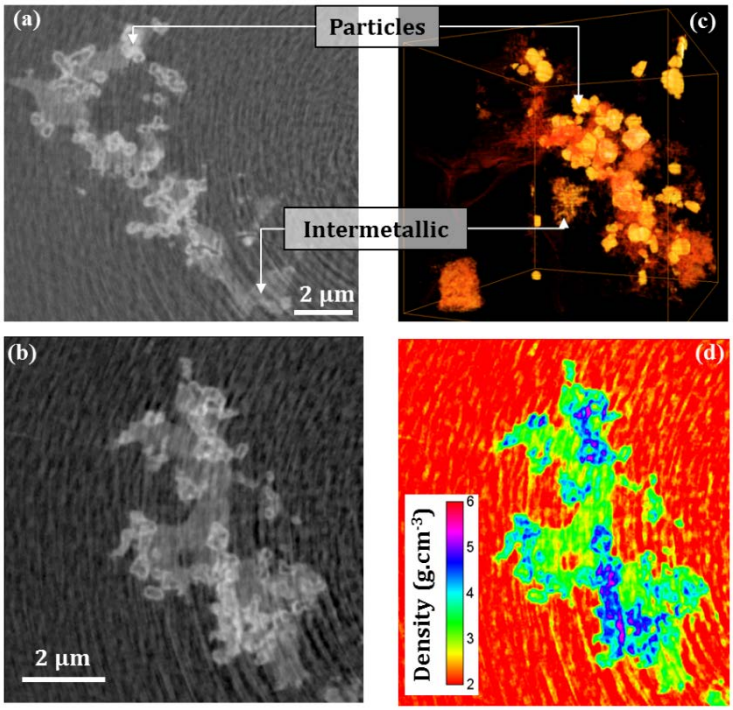

Figure 5 : (a) and (b) 2D Holo-nanotomography slices of the EL21+AlN composite (voxel size 25 nm) focusing on the intermetallic locations where particles can be seen. (c) 3D rendering of a similar area where particles can be found gathered in 3D in the intermetallic phase. (d) False colours density rendering of 2D slice (b). Pure Mg is red (1.8 g.cm^{-3}) and the intermetallic Mg_3-(Nd,Gd) is green (3.6 g.cm^{-3}) which reveals core-shell structure of Zr in pink (5.8 g.cm^{-3}) coated by Al_3Zr in dark blue (4.1 g.cm^{-3}).

The 3D rendering of a similar area is shown on Figure 5 (c) confirming that we are in presence of isolated aggregates of particles and not a modified crooked structure of the intermetallic phase. Moreover, as the holotomography technique uses the information of phase contrast, it is sensitive to the density of the phases inside the sample [37]. Therefore the grey level values of Figure 5 (b) can be converted into colours rendering related to the density. The α-Mg primary phase (1.8 g.cm^{-3}) thus appears in red and the intermetallic phase of composition Mg_3-(Nd,Gd) in green (3.6 g.cm^{-3}). Such colour-density equalizing procedure makes possible the identification of the core-shell structure of the particles present in the intermetallic phase. Surprisingly, the inner part of the aggregates is denser than the outer part. Indeed, the density values suggest that Zr (5.8 g.cm^{-3} in pink) is coated by Al_3Zr (4.1 g.cm^{-3} in dark blue) whereas it has been suggested by STEM-HAADF that Zr would be more prone to

surround AlN particles [14]. While the reactional sequence remains quite uncertain, the present data confirm that the addition of AlN particles leads to the modification of the local chemistry by reaction with Zr implying a modification of the intermetallic microstructure and is hence partially responsible of the improvement of the mechanical properties at high temperature as well as of the modification of the hardness inside the grains. Unfortunately, even if isolated AlN nanoparticles remain in the sample, even such a remarkable technique can not reveal them. First because their size is of the order of the pixel size which leave them lost in the background noise and second because their density is comparable to the one of the intermetallic phase (3.1 $g.cm^{-3}$) that also makes them invisible if they end up in this area. However, according to the TEM results [25], the AlN particles are more likely situated inside, or close to, the intermetallic phase confirming their tendency to be pushed by the solidification front during casting.

3.3. Discussion

In the light of these results, it is believed that the mechanical improvements, that at first sight could have been attributed to a direct strengthening (mainly by the creation of geometrically necessary dislocations) due to the present of the AlN nano-particles in the grains [5], originates more probably from indirect effects. Indeed, the creep compression tests indicate through the value of the Norton coefficient (n = 4.2, Figure 1) that creep is controlled by dislocation mechanisms and the increase of the threshold stress observed suggests that the resistance to the motion of dislocations is more important in the material with particles. Obstacles such as the dislocation themselves (forest strengthening), grain boundaries, particles or intermetallics can contribute to this threshold stress. The lower hardness values measured inside the grains of the material with particles (Figure 2) suggests that the contribution of the presence of particles (forest and Orowan), or precipitates [25], within grains is negligible. The amount of intermetallics as well as the grain size [25] are similar in both materials, however, the density of grain boundaries is higher in the composite and the morphology of the interdendritic phase (intermetallics) is different (Figure 3). Divers mechanisms can be proposed to explain these observations. First, the nano-particles can probably act as potent nucleation sites triggering the early formation of dendrites and thus modifying the solidification kinetics. Second, the particles can possibly interact with the solidification front by disturbing the solute concentration ahead of the advancing interface resulting in a more branched structure of grains [38] and eventually of the interdendritic phase. Also, the AlN particles were shown to react, at least partially, with the Zr contained in the El21 alloy (Figure 4 and 5) which implies a local variation of the chemistry as well as a modification of the very nature of the particles themselves. Finally, the presence of numerous and chemically different nano-particles inside the shape-modified interdendritic area can also play a role of reinforcement of the intermetallic phase itself.

4. Conclusions

The present paper reports the successful processing of an El21+AlN nano-composite where the obtained microstructure is nearly free of pores. The mechanical properties of the El21+AlN nano-composite at high temperature are enhanced by a factor 20 to 60 % compared

to the unreinforced material without detrimental effects on other mechanical properties at room temperature [25]. At the same time, nano-indentation tests performed inside the Mg primary grains suppose that no relevant effects on the motion of dislocations can be attributed to the presence of the AlN nano-particles or of potential precipitates [25]. Combining several complementary microstructural characterization techniques with previous results from Katsarou *et al* [25], we demonstrate that the AlN nanoparticles can greatly impact the final microstructure morphology, this latter presenting modified grain shapes and a more tortuous structure of the intermetallic phase. They also impact the local chemistry by reaction with Zr and are found located inside the interdendritic area. Such scenario indicates that the improvement of the mechanical response of the El21+AlN material at high temperature does not arise from the expected composite effect (forest strengthening) but rather from a more complex modification of the casting conditions leading to a different microstructure.

It highlights that careful analysis and deep investigation of the physical and chemical mechanisms at play during processing are mandatory to understand enhancements of mechanical properties and ultimately to design novel performant MMNCs. To go further, it would be compelling to model the deformation of a two phases material enacting the matrix-intermetallic distribution and compute the mechanical responses to evaluate in which extent the shape and the chemistry of the intermetallic phase influence the overall mechanical response.

Acknowledgment

The authors wish to acknowledge financial support from the ExoMet Project, which is co-funded by the European Commission in the 7th Framework Programme (contract FP7-NMP3-LA-2012-280421), by the European Space Agency and by the individual partner organizations.

They also wish to acknowledge the ESRF-MA1876 long term project, the ID19 as well as the ID16A beamline staff.

References

[1] Z. Yang, J.P. Li, J.X. Zhang, G.W. Lorimer, J. Robson, Review on Research and Development of Magnesium Alloys, Acta Metall. Sin. Engl. Lett. 21 (2008) 313–328. doi:10.1016/S1006-7191(08)60054-X.

[2] S. Tekumalla, S. Seetharaman, A. Almajid, M. Gupta, Mechanical Properties of Magnesium-Rare Earth Alloy Systems: A Review, Metals. 5 (2014) 1–39. doi:10.3390/met5010001.

[3] H.Z. Ye, X.Y. Liu, Review of recent studies in magnesium matrix composites, J. Mater. Sci. 39 (2004) 6153–6171.

[4] M. Taya, Strengthening Mechanisms of Metal Matrix Composites, Mater. Trans. JIM. 32 (1991) 1–19. doi:10.2320/matertrans1989.32.1.

[5] J.B. Ferguson, F. Sheykh-Jaberi, C.-S. Kim, P.K. Rohatgi, K. Cho, On the strength and strain to failure in particle-reinforced magnesium metal-matrix nanocomposites (Mg MMNCs), Mater. Sci. Eng. A. 558 (2012) 193–204. doi:10.1016/j.msea.2012.07.111.

[6] L. Ceschini, A. Dahle, M. Gupta, A.E.W. Jarfors, S. Jayalakshmi, A. Morri, F. Rotundo, S. Toschi, R.A. Singh, Aluminum and Magnesium Metal Matrix Nanocomposites,

Springer Singapore, Singapore, 2017. http://link.springer.com/10.1007/978-981-10-2681-2 (accessed January 20, 2017).
[7] M. Gupta, W.L.E. Wong, High Performance Magnesium Based Composites Containing Nano-Length Scale/Amorphous/Hollow Reinforcements, Mater. Sci. Forum. 879 (2017) 642–647. doi:10.4028/www.scientific.net/MSF.879.642.
[8] Z. Zhang, D.L. Chen, Consideration of Orowan strengthening effect in particulate-reinforced metal matrix nanocomposites: A model for predicting their yield strength, Scr. Mater. 54 (2006) 1321–1326. doi:10.1016/j.scriptamat.2005.12.017.
[9] L. Chen, Y. Yao, Processing, Microstructures, and Mechanical Properties of Magnesium Matrix Composites: A Review, Acta Metall. Sin. Engl. Lett. 27 (2014) 762–774. doi:10.1007/s40195-014-0161-0.
[10] H. Dieringa, Properties of magnesium alloys reinforced with nanoparticles and carbon nanotubes: a review, J. Mater. Sci. 46 (2010) 289–306. doi:10.1007/s10853-010-5010-6.
[11] S.F. Hassan, Effect of primary processing techniques on the microstructure and mechanical properties of nano-Y2O3 reinforced magnesium nanocomposites, Mater. Sci. Eng. A. 528 (2011) 5484–5490. doi:10.1016/j.msea.2011.03.063.
[12] M. Paramsothy, S.F. Hassan, N. Srikanth, M. Gupta, Enhancing tensile/compressive response of magnesium alloy AZ31 by integrating with Al2O3 nanoparticles, Mater. Sci. Eng. A. 527 (2009) 162–168. doi:10.1016/j.msea.2009.07.054.
[13] M. Habibnejad-Korayem, R. Mahmudi, W.J. Poole, Enhanced properties of Mg-based nano-composites reinforced with Al2O3 nano-particles, Mater. Sci. Eng. A. 519 (2009) 198–203. doi:10.1016/j.msea.2009.05.001.
[14] D. Zhou, F. Qiu, Q. Jiang, Simultaneously increasing the strength and ductility of nano-sized TiN particle reinforced Al–Cu matrix composites, Mater. Sci. Eng. A. 596 (2014) 98–102. doi:10.1016/j.msea.2013.12.049.
[15] S. Sankaranarayanan, M.K. Habibi, S. Jayalakshmi, K.J. Ai, A. Almajid, M. Gupta, Nano-AlN particle reinforced Mg composites: microstructural and mechanical properties, Mater. Sci. Technol. 31 (2015) 1122–1131. doi:10.1179/1743284714Y.0000000686.
[16] S.F. Hassan, M.J. Tan, M. Gupta, Development of nano-ZrO2 reinforced magnesium nanocomposites with significantly improved ductility, Mater. Sci. Technol. 23 (2007) 1309–1312. doi:10.1179/174328407X236913.
[17] S.F. Hassan, M. Gupta, Development of nano-Y2O3 containing magnesium nanocomposites using solidification processing, J. Alloys Compd. 429 (2007) 176–183. doi:10.1016/j.jallcom.2006.04.033.
[18] S.F. Hassan, M. Gupta, Development of high performance magnesium nanocomposites using solidification processing route, Mater. Sci. Technol. 20 (2004) 1383–1388. doi:10.1179/026708304X3980.
[19] W.H. Sillekens, D.J. Jarvis, A. Vorozhtsov, V. Bojarevics, C.F. Badini, M. Pavese, S. Terzi, L. Salvo, L. Katsarou, H. Dieringa, The ExoMet Project: EU/ESA Research on High-Performance Light-Metal Alloys and Nanocomposites, Metall. Mater. Trans. A. 45 (2014) 3349–3361. doi:10.1007/s11661-014-2321-2.
[20] A. Kielbus, T. Rzychon, Mechanical and creep properties of Mg-4Y-3RE and Mg-3Nd-1Gd magnesium alloy, Procedia Eng. 10 (2011) 1835–1840. doi:10.1016/j.proeng.2011.04.305.
[21] T. Rzychoń, A. Kiełbus, J. Cwajna, J. Mizera, Microstructural stability and creep properties of die casting Mg–4Al–4RE magnesium alloy, Mater. Charact. 60 (2009) 1107–1113. doi:10.1016/j.matchar.2009.05.014.
[22] T. Rzychoń, A. Kiełbus, L. Lityńska-Dobrzyńska, Microstructure, microstructural stability and mechanical properties of sand-cast Mg–4Al–4RE alloy, Mater. Charact. 83 (2013) 21–34. doi:10.1016/j.matchar.2013.06.001.

[23] A. Kielbus, Microstructure and mechanical properties of Elektron 21 alloy after heat treatment, J. Achiev. Mater. Manuf. Eng. 20 (2007) 127–130.
[24] M. Qian, D.H. StJohn, M.T. Frost, Zirconium alloying and grain refinement of magnesium alloys, Magnes. Technol. 2003 (2003) 209–214.
[25] L. Katsarou, M. Mounib, W. Lefebvre, S. Vorozhtsov, M. Pavese, C. Badini, J.M. Molina-Aldareguia, C.C. Jimenez, M.T. Pérez Prado, H. Dieringa, Microstructure, mechanical properties and creep of magnesium alloy Elektron21 reinforced with AlN nanoparticles by ultrasound-assisted stirring, Mater. Sci. Eng. A. 659 (2016) 84–92. doi:10.1016/j.msea.2016.02.042.
[26] S. Terzi, R. Daudin, J. Villanova, P. Srirangam, P. Lhuissier, L. Salvo, E. Boller, R. Schweins, P. Lindner, J.-J. Blandin, P. Lee, H. Lemmel, X-Ray Tomography and Small-Angle Neutron Scattering Characterization of Nano-Composites: Static and In Situ Experiments, in: J. Grandfield (Ed.), Light Met. 2014, John Wiley & Sons, Inc., 2014: pp. 1389–1393. http://onlinelibrary.wiley.com/doi/10.1002/9781118888438.ch232/summary (accessed March 23, 2015).
[27] M. Mounib, M. Pavese, C. Badini, W. Lefebvre, H. Dieringa, Reactivity and Microstructure of Al_2O_3-Reinforced Magnesium-Matrix Composites, Adv. Mater. Sci. Eng. 2014 (2014) e476079. doi:10.1155/2014/476079.
[28] H. Fang, C.D. Versteylen, S. Zhang, Y. Yang, P. Cloetens, D. Ngan-Tillard, E. Brück, S. van der Zwaag, N.H. van Dijk, Autonomous filling of creep cavities in Fe-Au alloys studied by synchrotron X-ray nano-tomography, Acta Mater. 121 (2016) 352–364. doi:10.1016/j.actamat.2016.09.023.
[29] V.C. Nardone, J.R. Strife, Analysis of the creep behavior of silicon carbide whisker reinforced 2124 Al(T4), Metall. Trans. A. 18 (1987) 109–114. doi:10.1007/BF02646227.
[30] E. Arzt, M.F. Ashby, Threshold stresses in materials containing dispersed particles, Scr. Metall. 16 (1982) 1285–1290. doi:10.1016/0036-9748(82)90484-7.
[31] J. Rösler, E. Arzt, The kinetics of dislocation climb over hard particles—I. Climb without attractive particle-dislocation interaction, Acta Metall. 36 (1988) 1043–1051. doi:10.1016/0001-6160(88)90158-7.
[32] E. Arzt, J. Rösler, The kinetics of dislocation climb over hard particles—II. Effects of an attractive particle-dislocation interaction, Acta Metall. 36 (1988) 1053–1060. doi:10.1016/0001-6160(88)90159-9.
[33] N. Chawla, Y.-L. Shen, Mechanical behavior of particle reinforced metal matrix composites, Adv. Eng. Mater. 3 (2001) 357–370.
[34] W.H. Sillekens, D. Casari, W.U. Mirihanage, S. Terzi, R.H. Mathiesen, L. Salvo, R. Daudin, P. Lhuissier, E. Guo, P.D. Lee, The Use of In Situ X-ray Imaging Methods in the Research and Development of Magnesium-Based Grain-Refined and Nanocomposite Materials, JOM. (2016) 1–9. doi:10.1007/s11837-016-2130-8.
[35] G. Requena, G. Garcés, M. Rodríguez, T. Pirling, P. Cloetens, 3D Architecture and Load Partition in Eutectic Al-Si Alloys, Adv. Eng. Mater. 11 (2009) 1007–1014. doi:10.1002/adem.200900218.
[36] R.E. Loehman, A.P. Tomsia, Reactions of Ti and Zr with AlN and Al2O3, Acta Metall. Mater. 40, Supplement (1992) S75–S83. doi:10.1016/0956-7151(92)90266-H.
[37] P. Cloetens, W. Ludwig, J. Baruchel, D. Van Dyck, J. Van Landuyt, J.P. Guigay, M. Schlenker, Holotomography: Quantitative phase tomography with micrometer resolution using hard synchrotron radiation x rays, Appl. Phys. Lett. 75 (1999) 2912. doi:doi:10.1063/1.125225.
[38] R. Daudin, S. Terzi, P. Lhuissier, J. Tamayo, M. Scheel, N.H. Babu, D.G. Eskin, L. Salvo, Particle-induced morphological modification of Al alloy equiaxed dendrites

revealed by sub-second in situ microtomography, Acta Mater. 125 (2017) 303–310. doi:10.1016/j.actamat.2016.12.005.